



Ship Technology Research >

Schiffstechnik

Volume 62, 2015 - Issue 1

Full access

1,454 14

Views

0

CrossRef citations to date | Altmetric



Lecture

Added resistance of ships in waves†

Heinrich Söding ✉ & Vladimir Shigunov

Pages 2-13 | Received 26 Mar 2014, Accepted 11 Dec 2014, Published online: 02 May 2015

Download citation <https://doi.org/10.1179/0937725515Z.00000000001>



Abstract

Added resistance of ships in waves is determined by a newly developed potential flow method, a Rankine source method, a strip method, and by RANS (Reynolds-averaged Navier-Stokes) equations solvers. For 10 ships, results of all these methods are compared with each other, with published computed and experimental results, and with approximation formulae submitted to IMO (International Maritime Organisation). The focus is on waves that are short relative to ship length. In spite of the large scatter of results, existing prediction methods appear useful for practical application.

Q Keywords: Added resistance Seakeeping Potential flow calculation

< Previous article

View issue table of contents

Next article >

Introduction

Because of high fuel cost, the added resistance of ships in waves contributes substantially to the operating cost of ships. Here moderate wave conditions are of main importance. Wave lengths in the range between 50 and 150 m contribute most to the average added resistance. Longer waves occur seldom because, roughly speaking, a wind of speed c does not excite waves the phase velocity of which exceeds c , and because wavelength λ is related to c and gravity acceleration g by

$$\lambda = 2\pi c^2 / g^1$$

Thus, for large ships the range of wavelengths $\lambda/L_{pp} < 0.5$ is of primary importance regarding fuel cost. However, the added resistance in seldom occurring, much longer and higher waves, can also be interesting because it may cause delays, either by allowing only reduced speed, or because a longer path is taken to circumvent the high seaway region.

Numerical field methods, such as finite-volume methods, are suitable to compute the added resistance; however,

because of their computational complexity they (and model experiments) are used mainly for verification of the much faster potential flow methods. The latter methods exist since about 50 years; however, substantial improvements have been made recently. Potential methods are applicable because viscosity does not contribute substantially to the added resistance.

The added resistance is the time average of the (negative) longitudinal force on a ship (or any other body) in waves minus the force in still water. Here the average motion of the ship (speed ahead, no drift angle, no rudder angle) is assumed the same with and without waves. This corresponds also to the majority of experimental procedures for measuring the added resistance.

Linear responses do not contribute directly to this force because their time average is zero. However, a good approximation to the added resistance results from products of pairs of linear responses. They constitute the second-order approximation. For the added resistance, three such products are of main importance:

- A. Pressure oscillations times normal vector on the hull; the latter oscillates because of the hull rotations in roll, pitch and yaw.
- B. Pressure oscillations times oscillations of the depth of hull immersion.
- C. Oscillations of the water velocity at the hull multiplied by itself. According to Bernoulli's equation, the squared velocity contributes to the pressure.

Added resistance can also occur because a bow bulb, which may be optimally submerged in still water, oscillates in waves between less favourable submergence values. Similar effects may be caused by the transom. Both effects are not accounted for by second-order methods.

In the following, three potential second-order methods for computing stationary (drift) forces and moments in regular waves (especially the added resistance) are discussed, and their results are compared with approximations submitted to IMO.

Rankine source method

The program *GL Rankine* uses, besides others, a three-dimensional Rankine source method described in Söding, el Moctar, von Graefe and Shigunov (2012); Söding, Shigunov, Schellin and el Moctar (2012); Söding, Shigunov, Schellin and el Moctar (2014). As a pre-requisite, this method needs the stationary flow and the stationary wave field around the body. Figure 1 shows this wave field for the tanker KVLCC2 ($L_{pp} = 320\text{m}$) computed by the patch method of the same program *GL Rankine*. The panel mesh on the body shown in Fig. 1 is used also to compute the flow in instationary waves; the free-surface panel mesh, on the other hand, is determined anew for each instationary wave condition. Thus the body panel mesh must be fine enough for the shortest wave when computing the stationary flow. This is the reason for using a much finer body mesh than the free-surface mesh in Fig. 1.

1. Free-surface and hull panel mesh and height contours of stationary waves around the KVLCC2 tanker in still water at $F_n = 0.18$

□

Display full size

Figures 2 and 3 show results in regular bow-quartering waves (wave direction 150° ; 180° correspond to head waves) for a smaller tanker ($L_{pp} = 260\text{m}$): heave and pitch motions; longitudinal and transverse drift force; and yaw drift moment. Curves show results of a coarse body panel mesh (maximum triangle side length $= L_{pp}/53$) and markers give

results of finer body panel meshes. The coarsest panel mesh is sufficient to produce mesh-independent motions, whereas for drift force and moment in higher frequencies finer meshes are required. Mesh-independent drift forces require, roughly, maximum body panel sides $\leq \text{wavelength}/25$.

2. Transfer functions for heave and pitch, computed by the Rankine source method for a tanker ($L_{pp} = 260\text{ m}$) in waves from direction 150° . Different body meshes: maximum panel size = $L_{pp}/53$ (curves), $L_{pp}/88$ (circles), $L_{pp}/115$ (squares) and $L_{pp}/133$ (asterisks)

□

Display full size

3. Transfer functions for longitudinal and transverse drift force and for yaw drift moment for the same case as in Fig. 2

□

Display full size

Three reasons are responsible for the fact that drift force and moment require finer meshes than linear responses:

- The product of two harmonic terms has a wavelength of size $1/2$ of the wavelength of the factors. This requires a proportionally finer panel mesh. A factor $1/2$ in the mesh size means a factor 16 in the number of elements of the matrix of the equation system for determining the source strengths. This limits the minimum wave height which can be handled appropriately by the method.
- In short waves, where the first of the three products listed above vanishes because the ship does not move, the two other products have opposite sign, thus cancelling each other to a large extent. If wavelength is short compared to the ship's draft, and if the stationary flow is neglected, the products 2 and 3 cancel exactly if the incoming wave is parallel to the hull, and they result in half of contribution 2 if the wave propagates normal to the hull.
- Whereas for linear responses in short waves, contributions of wave trough and wave crest cancel each other approximately, in second-order responses both contributions have the same sign. This is obvious in Figs. 2 and 3: for higher wave frequency motions tend to zero, but drift force and moment do not.

In the following, the added resistance R_{add} is characterised by the non-dimensional quantity

$$\frac{R_{add}}{\rho g \zeta_A B^2}$$

where ζ_A is the wave amplitude and B the ship's breadth. Figure 4 compares computed and measured values of C_{add} for the tanker KVLCC2 in head waves for two Froude numbers. The measured values published for this ship appear more reliable than usual. The values computed by the Rankine source method appear too small in short waves (for $\zeta_A/B > 0.5$). For the higher Froude number, using the double-body approximation for the stationary base flow causes noticeable inaccuracies.

4. Non-dimensional added resistance in head waves of various lengths for the tanker KVLCC2. Curves computed with the Rankine source method using, for the stationary flow, the double-body approximation (dotted) or the free-surface flow (continuous line); markers show results of model experiments in Bingje and Steen (2010) (circles) and according to Gothenburg Workshop (2010) (squares)

□

Display full size

For the cases shown in Fig. 4, Söding *et al.* (2012b) show better coincidence of computations with measured data. The computations used an earlier version of the same program. It had to be changed because of deficiencies in other cases, in spite of the better comparison in this case.

Strip method *PDStrip*

Figure 5 presents the same measured values as Fig. 4; the curves, however, show results of the strip method *PDStrip* (Bertram and Söding 2007, using the current (improved) version of this method. Here the maximum of the computed added resistance appears too large compared to the experimental data and to the results of the Rankine source method.

5. Like Fig. 4. but curves computed using the strip method *PDStrip*

□

Display full size

In waves shorter than about $0.8L_{pp}$ *PDStrip* gives too small values for the added resistance. It appears impossible to correct this within a strip method, because strip methods neglect longitudinal velocities of the diffraction flow. Together with the high sensitivity of drift forces this leads to the inability of the strip method to give correct drift forces in shorter waves in which first-order responses are computed approximately correct.

Lee method

Lee (1982) published another potential method to determine the added resistance. It is applicable to short waves in which periodic ship motions are negligible, and to waves from forward directions only. Motivated by the smaller computer power at that time, Lee approximates the dependence of the flow potential on the vertical coordinate z by the function e^{-kz} , where k is the wave number of the incoming wave. Lee solves for the flow potential in regular waves in the time domain, stopping the simulation before reflected waves reach the body.

Today, with more computer power available, one can use the approximation of the flow dependence on z to use finer panel meshes on the free surface, and to deal with shorter waves compared to other methods. Therefore, as an alternative for short waves, a method using, in principle, the same approximation for the dependence of the flow potential on z is developed. It reduces the three-dimensional flow problem to a two-dimensional one. However, instead of solving an instationary flow problem, the complex amplitudes of the free-surface height oscillations and of the periodic potential are determined.

Because the fully developed periodic flow is computed, a damping must be used to avoid reflections of diffraction waves from the outer boundary of the panel mesh on the free surface.

Lee approximates the stationary flow around the ship by a parallel flow. To improve the accuracy, now the correct stationary flow field and the stationary ship waves are used. The incoming waves are approximated by the Airy potential, i.e. by the linearised wave potential in parallel flow. Owing to the stationary flow field around the ship, the wave number of diffraction waves, which have the same encounter frequency as the incoming waves, depends on both location and wave propagation direction. Whereas the dependence on location does not cause problems, the dependence on propagation direction is problematical because, at the same location, waves of different directions are present. Thus reasonable approximations of the local wave number have to be made.

Conditions at free surface

In a free-surface region around the body, the flow potential Φ and the surface depression Z shall be determined. Both quantities consist of a stationary part (upper index 0) and a periodic part (upper index 1) oscillating with encounter frequency ω_e

$$\square 3$$

The kinematic condition of vanishing flow through the free surface is

$$\square 4$$

and the dynamic condition of constant pressure is

$$\square 5$$

Here g is the gravity acceleration, and u is the ship speed. Indices x and y designate partial derivatives with respect to longitudinal and transverse coordinates, respectively, in an inertial coordinate system proceeding with the average ship speed. The z -axis points downward.

Inserting for Φ and Z the expressions given in equation (3) results in

$$\square 6$$

and

$$\square 7$$

The stationary fields Φ^0 and Z^0 alone satisfy these equations. Therefore, terms containing only stationary quantities can be omitted. Further, second-order terms (containing squares or products of periodic quantities) are omitted. This results in

$$\square 8$$

$$\square 9$$

The periodic fields Z^1 and Φ^1 are splitted into known contributions $\zeta;^w, \phi^w$ from the incoming wave, and an unknown rest $\zeta;, \phi$ because of wave diffraction. This splitting is necessary because diffraction waves, but not incoming waves, must be damped to avoid reflections at the outer boundary of the discretised part of the free surface. This splitting is helpful also in other cases (see, e.g., Ferrant, Gentaz and Le Touzé, 2002).

Airy wave theory gives the following formulae for $\zeta;^w$ and ϕ^w

$$\square 10$$

$$\square 11$$

Here c_0 is the phase velocity of the incoming wave,

$$\square 12$$

and μ is the wave direction. Symbols with lower index 0 designate values for the parallel flow with speed $-u$ relative to the ship.

The encounter frequency ω_e is the same at all locations. It is related to the wave number k

$$\square 13$$

This equation shows a substantial drawback of the present method: ω and k depend on the wave propagation angle μ . It cannot be determined uniquely because, at the same location, waves of different directions are superimposed. Consider, for example, the midship part of the waterline on the luff side of the body. Here incoming waves of direction μ are superimposed to diffraction waves of direction $-\mu$. Because here \square , the same ω_e results both for incoming and diffraction waves. In the bow region, however, where \square different ω_e values result for incoming and diffracted waves, and the diffraction consists of waves of different directions and thus different ω and k . In the following, two approximations will be used:

- The steady potential Φ^0 is substituted by the parallel flow potential $-ux$. This is the condition used in Lee (1982).
- In equation (13) the term \square is omitted, and for μ , the direction of the incoming wave is used.

Splitting Z^1 and Φ^1 into contributions of incoming wave and diffraction allows to re-write equations (8) and (9) as follows

$$\square 14$$

$$\square 15$$

respectively. Here ∇ designates the two-dimensional nabla operator

$$\square 16$$

Because of the term \square , the two equations cannot be combined to a single equation of one variable field. Therefore, both ζ_i and ϕ are taken as unknowns.

The stationary flow field, which is determined previously by a stationary Rankine source method, is described by Z^0 and Φ^0 at free-surface grid points. \square is determined from the kinematic boundary condition as

$$\square 17$$

Also the z derivative of the diffraction potential ϕ must be substituted by values at the free surface. The combined periodic potential $\phi + \phi^w$ is supposed to be proportional to e^{-kz} . Thus

$$\square 18$$

This approximation appears suitable for equation (15). In equation (14), on the other hand, a stronger coupling to the potential at neighbour points on the free surface appears necessary. This was found already in Lee (1982). To derive a suitable expression, the z derivative of equation (18) is formed. It contains ϕ_{zz} . This is substituted using the three-dimensional Laplace equation, giving

$$\square 19$$

which results in

$$\square 20$$

Here Δ is the 2-d Laplace operator. Equation (20) does not hold exactly because of the change of k with location and because of the curvature of the stationary water surface. The approximation is good if the wavelength is small compared to the length scale in which the stationary flow field changes substantially.

Using the above substitutions in equations (14) and (15) results in the following two conditions

$$\square 21$$

$$\square 22$$

The time derivatives of the incoming wave fields ζ_i^w and ϕ^w are

$$\square 23$$

$$\square 24$$

respectively. Thus, one obtains the partial time derivatives of ζ_i and ϕ in the form

$$\square 25$$

$$\square 26$$

respectively. The last term in equation (26) was added here to generate artificial damping of the diffraction waves. The factor α determines the magnitude of damping; it is taken as small (0.01) near to the body and increasing quadratically with distance from the body.

Boundary conditions

In an unpublished investigation (Söding 2013), it was shown that the drift force on a vertical plane wall intersecting the water surface is the same as that on an inclined wall. Therefore, the hull is assumed here as vertical in the waterline. This gives the boundary condition

$$\square 27$$

where \square is the horizontal normal vector to the stationary waterline. From equations (8), 9 and (27)) follows the corresponding condition for $\zeta_i + \zeta_i^w$.

At the outer boundaries of the discretised free surface, the normal derivatives of ζ ; and ϕ are set to zero. This causes reflections of the diffraction waves; however, because of the artificial damping, the waves are negligible there.

Approximation of space derivatives

Figure 6 shows part of the computational grid at the free surface; Fig. 7 shows an example of the total grid. Transverse mesh lines are in planes $y = \text{constant}$. In the finite-difference method applied here, y derivatives of a function $f(x, y)$ are approximated as (compare Fig. 6)

$$\frac{\partial f}{\partial y} \approx \frac{f_3 - f_1}{2\Delta y} \quad (28)$$

whereas x derivatives are computed as

$$\frac{\partial f}{\partial x} \approx \frac{f_2 - f_4}{2\Delta x} \quad (29)$$

To satisfy the boundary condition at the waterline, we need function values f_4 such that

$$\frac{\partial f}{\partial x} = 0 \quad (30)$$

Approximating f between points 4 and 6 by a second-order polynomial gives

$$f(x) = a_0 + a_1x + a_2x^2 \quad (31)$$

The x derivative is determined analogous to equation (29) as

$$\frac{\partial f}{\partial x} = 2a_2x + a_1 \quad (32)$$

The normal vector on the waterline at point 4 is approximated as

$$\mathbf{n} = (n_x, n_y) \quad (33)$$

where $i_r = 1$ on starboard and -1 on port side. From these equations follows the value f_4 satisfying the condition $\frac{\partial f}{\partial x} = 0$ as

$$f_4 = \frac{f_1 + f_3}{2} \quad (34)$$

Corresponding simple approximations of the Laplace operator $\Delta f = f_{xx} + f_{yy}$ were found to be too inaccurate. Thus, Δf at point 5 is determined by approximating f in the patch of Fig. 6 as a polynomial of degree 2 in x and y

$$f(x, y) = a_0 + a_1x + a_2y + a_3x^2 + a_4xy + a_5y^2 \quad (35)$$

As the formula contains only six unknowns, the method of minimum weighed errors is used, applying weights corresponding to Simpson's rule: 0.25 at points 1, 3, 7 and 9; 1 at points 2, 4, 6 and 8; and 4 at point 5. From equation (35) follows

$$\Delta f = 6a_3 + 2a_5 \quad (36)$$

6. Part of the free-surface grid

□

Display full size

7. Panel mesh around a tanker ($L_{pp} = 260\text{m}$) in waves of length 86 m from 150° . Height contours differing by $\Delta z = 0.1\text{ m}$ at $t = 0$ for incoming wave plus diffraction, excluding stationary waves

□

Display full size

Solving for ζ and ϕ

The time-periodic quantities ζ and ϕ are characterised by their complex amplitudes

$$\zeta = \zeta_0 e^{i(\omega t - kx)} \quad (37)$$

$$\phi = \phi_0 e^{i(\omega t - kx)} \quad (38)$$

Entering these expressions into the field equations (25) and (26) and into the boundary conditions gives a linear equation system for ζ_0 and ϕ_0 at all free-surface grid points. The coefficient matrix of the system has a band structure with a maximum band width of $2N_B + 5$, where N_B is the number of mesh points on a single transverse mesh line. The system is solved by elimination using a subroutine of the Lapack package.

Determination of drift force

If, because of small wavelength, the body does not move periodically, only effects 2 and 3 listed in the introduction are responsible for the drift force. The product of oscillations of pressure and immersion causes the following time-averaged (drift) force per waterline length (positive direction is into the body)

$$\square 39$$

Here the overbar designates the time average. a is the vertical acceleration of water particles because of stationary flow along the waterline

$$\square 40$$

The square of the periodic velocity contributes a 'Bernoulli force' per length

$$\square 41$$

The integral is taken along the section between $z=0$ (the difference between ζ_i and 0 is of higher order and thus negligible) and the section draft T . Assuming that the velocities decrease with depth proportional to e^{-kz} results in

$$\square 42$$

Further remarks

In the dynamic free-surface condition, it would be more accurate to substitute the quantity g by \bar{g} like it was done in determining the drift force. However, because the influence of a on the drift force was found to be small ($\leq 2\%$) in equation (39), it was neglected in equation (26).

The factor \square in equation (42) takes account of the finite draft of the body. A similar factor would be appropriate to modify the wave reflection at the waterline; however, this was also neglected.

Estimation formulae for added resistance in short waves

Tsujimoto, Kuroda, Shibata and Takagi (2008) proposed a method to estimate the added resistance in regular waves. The method is also discussed for application in IMO (2013). Here the version of the method is applied, which is recommended in short waves if no experimental data are available. It uses the formula

$$\square 43$$

where B_f is a waterline bluntness coefficient (it depends also on wave angle μ), α_T takes account of the ship draft, and C_U accounts for the influence of speed. For details see the cited IMO paper.

Further, the above named IMO paper gives a simplified formula for the resistance in a natural seaway if ship motions are negligible (Chapter E3, page 59)

$$\square 44$$

The formula is described as applicable in the range $135^\circ \leq \mu \leq 225^\circ$. It can be converted into one for regular waves if one assumes that R_{add}/\square does not depend on wave frequency. (The formula contains no characteristic period.) Using the relations

$$\square 45$$

where m_0 is the variance of the surface height, and

$$\square 46$$

one obtains the following formula for added resistance in regular waves from forward directions

$$\square 47$$

Results for a tanker

Figures 7 and 8 show the panel mesh and the real part of the complex amplitude of the periodic free surface elevation (incoming wave+diffraction) around the smaller tanker ($L_{pp} = 260\text{m}$). In front of the bow short waves occur. Resolving them requires a fine panel mesh which is not feasible when using the Rankine source method.

8. Zoomed bow area of Fig. 7

□

Display full size

Figure 9 corresponds to Figs. 4 and 5; however, here the curves show results of the Lee method. Their extent illustrates the range of wavelengths in which the method is applicable. A and B designate the variants explained in the section Conditions at the Free Surface. In the following, only variant B is used.

9. Non-dimensional added resistance in head waves of various lengths L_w for tanker KVLCC2. Curves computed by the Lee method (variants A and B); marker: experimental values like in Fig. 4; dotted lines according to approximations equation (43) (narrow) and equation (47) (wide)

□

Display full size

Results for a containership

Figures 10 and 11 show similar comparisons for the container ship used in the project Wave-Induced Loads on Ships (WILS), further referred to as WILS ship ($L_{pp} = 321\text{ m}$) (Hong 2011). Results computed by means of the Rankine source method (R) and the Lee method (LB) are plotted as curves. Markers indicate results computed using a RANS method (Fig. 10) and experimental values (Fig. 11). Whereas the results of the Rankine source method appear too small for the KVLCC2 tanker when wavelength is close to ship length, they appear rather large here, especially when compared with the experimental results. Further, Figs. 10 and 11 demonstrate the large difficulties encountered in the experiments as well as in all kinds of computations for small wavelengths. At the moment it appears impossible to decide which of the methods gives approximately correct results.

10. Non-dimensional added resistance in head waves of various lengths L_w for the WILS containership. Curves computed by the Rankine source (R) and variant B of the Lee method (LB). Marker according to RANS computations (Söding *et al.* 2012) using a coarse (squares) and a fine (circles) mesh. Dotted lines according to approximations by equations (43) (narrow) and (47) (wide)

□

Display full size

11. Corresponds to Fig. 10, but here markers show results of model experiments evaluated by two different methods

□

Display full size

Comparing results for the KVLCC2 tanker (Fig. 4) with those for the WILS containership (Figs. 10 and 11), moderate relative differences of C_{add} are found in the region of maximum response, but very large relative differences (factor 2

to 5) between the tanker and the containership in short waves. The ratio between added resistance for both ships is even larger because C_{add} contains the squared breadth B in the denominator, and because the tanker ($L_{pp}/B = 5.53$) has greater breadth than the containership ($L_{pp}/B = 6.63$). Still more pronounced is the relative increase in fuel consumption due to the seaway because the slow tanker requires much less power in still water than the faster container vessel.

Figure 12 shows the dependence of the non-dimensional added resistance on wave direction relative to the ship. Whereas stern (0°) and quartering waves push the ship a little, between 120° and 180° the added resistance is nearly constant. In other cases, the added resistance in head waves is smaller than that between 120° and 150° .

12. Non-dimensional added resistance for tanker KVLCC2 at $F_n = 0.18$ versus wave angle for wavelength $L_{pp}/3$, computed using Rankine source method (continuous line) and the Lee method, variant B (broken line)

□

Display full size


Results for other ships

Because methods for determining added resistance in short waves, including experiments and RANS calculations, appear questionable, a comparison of results for several other ships is worthwhile. Table 1 shows main data of ships; Fig. 13 shows C_{add} for ships A to J plotted over θ . Continuous curves correspond to Rankine source method, broken curves to Lee method B, narrowly dotted to equation (43) and widely dotted to equation (47). Symbols \circ correspond to asymptotic formula (Faltinsen, Minsaas, Liapis and Svein 1980) and squares for ships B, D and I correspond to RANS simulations by T. Zorn, DNVGL. Experiments are shown for Ship A as \square (Bingje and Steen 2010) and \square (Gothenburg Workshop 2010); for Ship C as $*$ (Ottosson and Brown 2012), for Ship H as $*$ (Pinkster 1980) and for Ship J as \square and \square (Hong 2011). For Ship A, squares correspond to RANS simulations (Sadat-Hosseini *et al.* 2013) and \circ to far-field method (Gerritsma and Beukelman 1972). For Ship B, \square corresponds to zero-speed Green functions method (Liu, Papanikolaou and Zaraphonitis 2011). For Ship J, small and large squares correspond to Euler- and RANS-based simulations (Walter 2011), respectively.

Table 1. Main dimensions of test ships

CSV

Display Table



13. C_{add} for ships A to J plotted over θ

□

Display full size

Results in natural seaway

All previous results were for regular waves. They allow to determine the added resistance in natural seaway by adding contributions from different wavelengths and directions. For the smaller tanker ($L_{pp} = 260$ m), Fig. 14 shows the result for various seaway directions and magnitudes. The latter are specified in Fig. 14 by the Beaufort number of the wind

generating the seaway after a sufficiently long time. Table 2 shows the seaway data used, depending on Beaufort number: the modal period T_p , the period T_1 corresponding to the centre of gravity of the area under the wave spectrum, and the significant wave height $h_{1/3}$.

14. Added resistance of the smaller tanker ($L_{pp} = 260\text{m}$) in natural fully developed seaway from various directions

□

Display full size

Table 2. Correlation between wind force and characteristic values of the seaway	
CSV	Display Table

Short-term data like those shown in Fig. 14 may be used to determine a long-term average of the added resistance. To that end, the short-term values are weighted by the frequency of occurrence of the seaway generating them. However, not fully developed seaways, which have a different relation between significant height and period and a different spectral shape, should also be included.

Here, a simpler method was used to approximate the long-term average added resistance of the smaller tanker in worldwide service: From Blendermann (2013), the median value of the wind velocity at 10m above the water surface in all oceans was found to be 7.89 m s^{-1} . (More sheltered regions are excluded.) The value is based on long-time satellite measurements of the roughness of the oceans published by Young and Holland (1996) for 126 locations. The distribution of wind velocity was assumed to be a Weibull distribution with exponent $c = 2$. This gives a modal (most frequent) wind velocity of

□ 48

The cumulative distribution of wind velocity over the oceans is then

□ 49

It gives the distribution of wind speed shown in Table 3.

Table 3. Assumed frequency distribution of wind speed over the oceans	
CSV	Display Table

The relation between wind speed and added resistance due to wind waves in head wind was taken from Fig. 14. It was inter- and extrapolated for the centre values of wind speed intervals of Table 3. Adding contributions from the different wind speed intervals weighted by their frequency of occurrence results in a mean added resistance in case of head wind of 119kN, i.e. 9% of the trial trip resistance. Averaging over all directions (assumed to be equally distributed) gives a mean added resistance in the open oceans of 4% of the trial trip resistance if the forward wave drift force in aft and quartering winds is neglected; otherwise it is 3.5%.

Conclusion

Computing drift forces, especially the added resistance, by potential methods appears not yet accurate, especially in waves of lengths $< 1/2$ of ship length. The same seems to hold for Euler and RANS computations and model experiments, although it cannot be excluded that some sets of field calculations and experiments may be accurate.

The strip method used here gave inaccurate results for added resistance for wavelengths exceeding $0.8L_{pp}$, and unacceptable results for shorter wavelengths. Therefore strip theory results were not included in Fig. 13.

The present Rankine source method and the Lee method appear, however, suitable to predict useful estimates of the added resistance even in short waves. Thus, they can be used to optimise main dimensions and block coefficient of ships including effects of the seaway, whereas experiments and RANS calculations appear too involved for this application.

The proposed IMO formula (43) appears approximately correct for full ships, whereas for more slender ships it seems to overpredict the added resistance in short waves. The proposal to IMO for natural seaway, equation (47), on the other hand, appears much too large in all cases. Especially, it gives approximately twice the values resulting from formula (43).

Whereas the Faltinsen formula for short waves gave reasonable values for the two ships to which it was applied, the Gerritsma method gave much too low values for the KVLCC2 tanker.

Because of fuel costs, and because of the IMO regulations regarding the Energy Efficiency Design Index, ship designers and operators are interested in means of reducing the fuel consumption. This can be achieved by reducing service speed, ship breadth and block coefficient. This reduces not only the resistance in still water, but also the added resistance in a seaway.

For large slender ships like panamax or post-panamax containerships, the average added resistance in waves appears negligible. Nonetheless, added resistance predictions may be necessary for the selection of main engine and propeller to ensure that the ship can fulfil contractual limitations in seaway, i.e. for a rational definition of the sea margin. This is especially relevant in case of slow steaming: Because added resistance in waves decreases much slower with decreasing ship speed than the calm-water resistance, the sea margin expressed as a percentage of calm-water power must be much higher in slow steaming than at a higher design speed.

Figure 14 shows that the added resistance increases rapidly with the Beaufort number Bft: The wind velocity is proportional to Bft. 1.5. For fully developed seaway, which is frequent in short waves because it requires small fetch and duration, significant wave height is proportional to wind velocity squared. The added resistance is proportional to significant wave height squared. Thus, for fully developed seaway the added resistance is proportional to Bft. 6. Therefore, small differences in Bft or significant wave height cause large differences in added resistance. Correcting trial power measurements for the influence of the seaway requires, thus, accurate seaway data. Visually estimated wave data appear hardly applicable for this purpose. To compute the seaway during a trial trip from the past and present wind field appears to be a viable alternative if no wave measurements are available.

[< Previous article](#) [View issue table of contents](#) [Next article >](#)

References

1. Bertram, V. and Söding, H. 2007. Verification of the *PDStrip* 2-d radiation problem module. In: 10-th Numerical Towing Tank Symp.. [\[Google Scholar\]](#)
2. Bingje, G. and Steen, S. 2010. Added resistance of a VLCC in short waves., In: Proceedings of 29-th International Conference on Ocean, Offshore and Arctic Engineering OMAE2010. Paper Nr. OMAE2010-20115.. [\[Google Scholar\]](#)

3. Blendermann, W. 2013. Practical ship and offshore structure aerodynamics. Hamburg: TUHH, Schriftenreihe Schiffbau, [ISBN 978-3-89220-669-9]. [\[Google Scholar\]](#)
4. Faltinsen, O. M., Minsaas, K. J., Liapis, N. and Svein, S. O. 1980. Prediction of resistance and propulsion of a ship in a seaway. In: Proceedings of 13-th Symposium on Naval Hydrodynamics, Tokyo.. [\[Google Scholar\]](#)
5. Ferrant, P., Gentaz, L. and Le Touzé, D. 2002. A new potential/RANSE approach for water wave diffraction. In: Proceedings of 5th NuTTS.. [\[Google Scholar\]](#)
6. Gerritsma, J. and Beukelman, W. 1972. Analysis of resistance increase in waves of a fast cargo ship. The journal International Shipbuilding Progress, 19(217), pp.285–93. [\[Google Scholar\]](#)
7. Gothenburg Workshop. 2010; Available at: < <http://www.gothenburg2010.org/kvlcc2.html>>. [\[Google Scholar\]](#)
8. Hong, S. Y. 2011. Wave induced loads on ships, Joint Industry Project WILS II. MOERI Techn. Rep. No. BSPIS503A-2207-2, Daejeon, Korea (confidential).. [\[Google Scholar\]](#)
9. IMO, 2013;. Additional information on revision of ISO 15016:2002. Paper MEPC 66/INF.7 submitted by ISO and ITTC. Annex, p. 51. [\[Google Scholar\]](#)
10. Lee, K. Y. 1982. Ein Beitrag zur Berechnung der Widerstandserhöhung in von vorn kommenden Wellen (A contribution to computing added resistance in head waves; in German). Hamburg: Institut für Schiffbau Hamburg, [Report No. 431]. [\[Google Scholar\]](#)
11. Liu, S., Papanikolaou, A. and Zaraphonitis, G. 2011. Prediction of added resistance of ships in waves. Ocean Engineering, 38(4), pp.641–50. [\[Crossref\]](#), [\[Web of Science ®\]](#), [\[Google Scholar\]](#)
12. Ottosson, P. and Brown, M. 2012. Captive tests for investigating manoeuvrability at low speeds, SSPA Rep. No. RE40105446-02-00-A. [\[Google Scholar\]](#)
13. Pinkster, J. A. 1980. Low frequency second order wave exciting forces on floating structures., Netherlands Ship Model Basin Wageningen, The Netherlands. [Publication No. 6501980].. [\[Google Scholar\]](#)
14. Sadat-Hosseini, H., Wu, P. -C., Carrica, P. M., Kim, H., Toda, Y. and Stern, F. 2013. CFD verification and validation of added resistance and motions of KVLCC2 with fixed and free surge in short and long head waves. Ocean Engineering, 59(1), pp.240–73. [\[Crossref\]](#), [\[Google Scholar\]](#)
15. Söding, H., el Moctar, B., von Graefe, A. and Shigunov, V. 2012a. Rankine source method for seakeeping predictions. In: Proceedings of 31-st International Conference on Ocean, Offshore and Arctic Engineering OMAE2012, June 10-15, Rio de Janeiro, Brazil. [Paper Nr. OMAE2012-83450].. [\[Google Scholar\]](#)
16. Söding, H., Shigunov, V., Schellin, T. E. and el Moctar, O. 2012b. A Rankine panel method for added resistance of ships in waves. In: Proceedings of 31-st International Conference on Ocean, Offshore and Arctic Engineering OMAE2012, June 10-15, Rio de Janeiro, Brazil. [Paper Nr. OMAE2012-83457].. [\[Google Scholar\]](#)

17. Söding, H. 2013. Welle und Wand (Wave and wall; in German), [private communication].. [\[Google Scholar\]](#)
18. Söding, H., Shigunov, V., Schellin, T. E. and el Moctar, O. 2014. A Rankine panel method for added resistance of ships in waves. *Journal of Offshore Mechanics and Arctic Engineering*, 136(3), pp.0316011–7. [\[Crossref\]](#), [\[Google Scholar\]](#)
19. Tsujimoto, M., Kuroda, M., Shibata, K. and Takagi, K. 2008. A practical correction method for added resistance in waves. *Journal of the Japan Society of Naval Architects and Ocean Engineers*, 8, pp.147–54. [\[Google Scholar\]](#)
20. Walter, S. 2011. Analysis of an approach to the definition of the added resistance of ships due to waves with RANSE methods. Dipl. Thesis, Univ. Duisburg-Essen.. [\[Google Scholar\]](#)
21. Young, I. R. and Holland, G. J. 1996. *Atlas of the oceans: wind and wave climate*. Pergamon: Oxford. [\[Google Scholar\]](#)

Related research

People also read

Recommended articles

Cited by
14

Duisburg Test Case: Post-Panamax Container Ship for Benchmarking >

Ould el Moctar et al.

Ship Technology Research

Published online: 2 Feb 2015



On the resistance and speed loss of full type ships in a seaway >

Shukui Liu et al.

Ship Technology Research

Published online: 7 May 2019



Resistance experiments and self-propulsion estimations of Duisburg Test Case at 1/100 scale >

Omer Kemal Kinaci et al.

Ship Technology Research

Published online: 28 Feb 2020



View more

Information for

Authors
Corporate partners
Editors
Librarians
Societies

Opportunities

Reprints and e-prints
Advertising solutions
Accelerated publication
Corporate access solutions

Keep up to date

Register to receive personalised research and resources by email



Sign me up



Open access

Overview
Open journals
Open Select
Dove Medical Press
F1000Research

Help and information

Help and contact
Newsroom
All journals
Books

Copyright © 2021 Informa UK Limited [Privacy policy](#) [Cookies](#) [Terms & conditions](#) [Accessibility](#)

Registered in England & Wales No. 3099067



Taylor & Francis Group
an informa business

In this article

